Effect of Electric Arc Furnace Slag on Nuclear Attenuation Properties of Smart Concrete

A.G. Asran[1], M.M. Sadawy[2], M. Nooman[3], A.A. Nada[4]

[1]Civil Engineering Department, Faculty of Engineering, Al-Azhar University, Nasr City, Cairo, Egypt.
[2]Mining and Petroleum Engineering Department, Al-Azhar University, Nasr City, Cairo 11371, Egypt.
[3]Civil Engineering Department, Faculty of Engineering, Al-Azhar University, Nasr City, Cairo, Egypt.
[4]Civil Engineering Department, Higher Technological Institute 10 Th. Of Ramadan city, Al Sharqiya, Egypt
Egy_scofield@yahoo.com

Abstract: A series of concrete mixes were prepared by replacement percentages 0, 5, 10, 15 and 20 wt% of cement by electric arc furnace slag (EAF).Mechanical tests and different types of nuclear radiation were used to evaluate the effect of slag on mechanical properties, the macroscopic neutron cross-sections (Σ,cm-1) and mass attenuation coefficients(σ, cm2/g) of gamma ray respectively. The results showed that, the mechanical properties of concrete increased with increasing electric arc furnace slag up to 15 wt. %. Moreover, 15 wt% mix sample was the optimum percentage for the values of mass attenuation coefficients of concrete maxis. On the other hand, there is no a significant variation of the values of Σ for all used neutron energy by adding a different percentage of slag as a cement in concrete.

[A.G. Asran, M.M. Sadawy, M. Nooman, A.A. Nada. **Effect of Electric Arc Furnace Slag on Nuclear Attenuation Properties of Smart Concrete.** N Y Sci J 2018;11(4):29-35]. ISSN 1554-0200 (print); ISSN 2375- 723X (online). http://www.sciencepub.net/newyork. 4. doi:10.7537/marsnys110418.04.

Keywords: Electric Arc Furnace Slag, Nuclear Attenuation Properties, Smart Concrete

1. Introduction

Radiation shielding concretes are commonly used in nuclear power plants, nuclear medicine facilities, and nuclear research facilities [1- 5]. With respect to the material for production of radiation shielding concretes, the guidelines in ACI 304R specify that magnetite, barite, and hematite in high ratios and colemanite and boron additives in low ratios should be used as the materials for the production of radiation shielding concretes. The guidelines from the International Commission on Radiological Protection (ICRP) are widely used as the standard for radiation shielding [6]. While materials with high-specific gravity are required for the shielding of gamma rays, materials such as water, boron, and graphite can be used for neutron radiation [7]. The radiation shielding property varies with the amount and type of concrete aggregates [8, 9]. Although magnetite or barite (density greater than 4.0 t/m3) have been used in previous studies [10, 11], they involve numerous problems pertaining to concrete manufacturing, such as low slump, low compressive strength, and material segregation of concrete. Various materials have been used in previous studies to alleviate these issues and develop radiation shielding concrete [12]. For example, research has been conducted on the development of concrete based on radiation shielding materials such as lead and iron [13- 15]. There have been studies on the effect of adding silica fume and blast furnace slag [16] on the attenuation coefficient [17], and a study on the development of radiation 47 shielding concrete based on the aggregates specific to each nation (e.g., stones or soil) [18, 19]. Much research has been conducted on high-density aggregates [20]. A few recent studies have focused on steel industry by-products [21, 22]. Although these by-products contain a large amount of recyclable and useful resources, current measures of disposal rely primarily on depositing them into landfills. With global attention to environmental problems, the practical applicability of industrial by- products is being researched [23]. Among steel slags, extensive research has been conducted on the recyclability of electric arc furnace (EAF) oxidizing slag [24]. While the use of EAF oxidizing slag is increasing with global advances in the steel industry, it is only used in road base and subbase, or hot mix asphalt, and is otherwise deposited in landfills, and no clear recycled use is known [25]. Research has been conducted to assess the possibility of developing concrete based on EAF oxidizing slag aggregates (EAF), the improvement effect of concrete on compressive strength, and the enhancement of durability [26- 28]. EAF oxidizing slag contains iron (15 – 30%), and has a high density of 3.0-3.7 t/m3. Therefore, it is believed that such high-density EAF can be used as an aggregate for radiation shielding concrete.

The objective of this research is to investigate the effect of arc furnace slag as cement replacement materials on mechanical and nuclear attenuation behaviors of concrete

2. Experimental Programmed Materials

Electric arc furnace (EAF)

Table 1 shows the chemical composition of EAF determined by XRF analysis. EAF contains around 35% iron and therefore has a high density. Thus, it is believed that the use of EAF for radiation-shielding concretes in place of cement will be highly effective.

Table 1 Chemical properties of the EFA (mass ratio, %)

SiO_2	Al_2O_3	Fe_2O_3	CaO	MgO	MnO	L.O.I
15	11	37	26	3	6	2

Ordinary Portland cement (OPC)

The present study was carried out using a commercial Portland cement type CEM I 42.5 N conforming to Egyptian standard code ESS 2421/2007. The physical, chemical and mechanical properties of this cement are given in Table. 2.

Table2 Properties of Cement Type (CEMI 42.5N)

Chemical	Composition (wt. %)	Physical properties	Compressive strength (N/mm2)
SiO_2	20.36	Fineness (cm2/gm) 3290	2 days 22.4
Al_2O_3	5.12	Specific Gravity 3.15	7 days 33.7
Fe_2O_3	3.64	Expansion (mm) 1.2	28 days 56.8
CaO	63.39		
MgO	1.03		
SO_3	2.21		
L.O.I	1.3		

Coarse and Fine Aggregates

Natural siliceous sand having a fineness modulus of 2.66 and a specific gravity of 2.67 was used as fine aggregate. The coarse aggregate was a crushed dolomite with a maximum nominal size of 18 mm with a specific gravity of 2.64 and a crushing modulus of 23 percent.

Mixing and casting

Concrete mixes were prepared using a tilting drum mixer. The weighted coarse and fine aggregates were placed in the mixer and started mixing for 30 seconds to obtain a homogeneous mix. The cementitious materials were added to the mixer and stirred for 2 min. The water was slowly added and mixed for 2 min. The mixing process was continued for 3 min. Under a laboratory conditions, six cubes of 150 mm and six cylinders of 150 × 300 mm were prepared. After casting, all specimens were covered with plastic sheet and stored in the laboratory for 24 hours. The specimens were then demolded, and placed in water for 28 days. Moreover, one of the prepared cylinder was cut off by thickness varies from 5 up to 20 cm for nuclear radiation (γ-rays and neutrons) measurements.

Fresh properties of concrete mixes

The consistency and workability of the concrete mixes was evaluated using the slump cone test.

Mechanical tests

Compressive strength tests on cubes at 7 and 28 days were carried out in a compression testing machine. The cubes were fitted and the load was slowly applied. The tensile strength tests were performed on cured cylinders specimen at 28 days.

Microstructure Analysis

X-ray diffraction (XRD, Philips Analytical X-ray B.V. Machine) and scanning electron microscope (SEM, Joel-JXA-840A) have been used to investigate the structure of concrete with and without blast furnace slag. All concrete samples were coated with gold to improve the appearance of microstructure.

Neutron and gamma ray measurements and calculations

The BF3 neutron detector was used to detect a collimated slow neutron, total slow neutron, and neutron with energy greater than 10 keV beam emitted from ^{241}Am-Be neutron source with activity 3.7 GBq. the neutron transmitted fluxes were measured according to equation (1) [29] to deduce the values of macroscopic neutron cross-section. In case of slow neutrons measurements, the collimated beam was slowed down by 7 cm polyethylene block behind the sample, also the neutron of energy below 10 keV was cut off by a block of Born carbide B4C. the Schematic diagram of experimental setup was shown in Fig.1.

$$I = I_o\, e^{-\Sigma x} \qquad \text{Eq (1)}$$

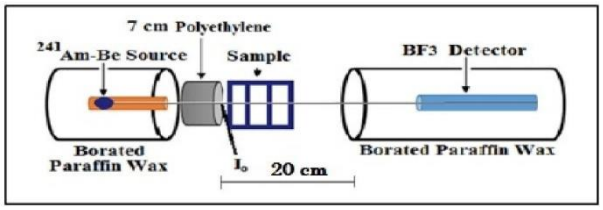

Fig.1: Schematic diagram of Neutron spectrometer

A collimated beam of gamma rays emitted from 3.7 μCiEu- 152, 9.5 μCi Cs-137, and 4.9 μCiCo-60 radioactive sources were used as sources of gamma ray energies. six pronounced peaks from the energy spectrum of gamma rays were chosen to cover a wide band of gamma energies to study the gamma ray attenuation coefficients of the investigated concrete barriers Fig.2 showed the schematic diagram of gamma ray detection system, where a 3″ x 3″ NaI (Tl) scintillation detector was used to measure the gamma ray intensities for the studied energy lines. The Beer- Lambert's equation was used to evaluate the linear attenuation coefficient, which considered the basic nuclear parameter, depending on the gamma ray intensities that transmitted from the investigated samples [30], [31].

$$\mu = \frac{\ln(\frac{I}{I_o})}{x}$$ Eq (2)

Where, Io & I are the intensities of gamma rays before and after transmitted the sample, respectively, μ (by cm^{-1}) is the linear attenuation coefficient of the sample, and x is the thickness of the sample. Mass attenuation coefficient, σ (by cm^2/g) is another important nuclear parameter which independent of density of the material, was evaluated from equation (3) after considering superficial density (xρ) in states of thickness.

$$\sigma = \frac{\ln(\frac{I}{I_o})}{x\rho}$$ Eq (3)

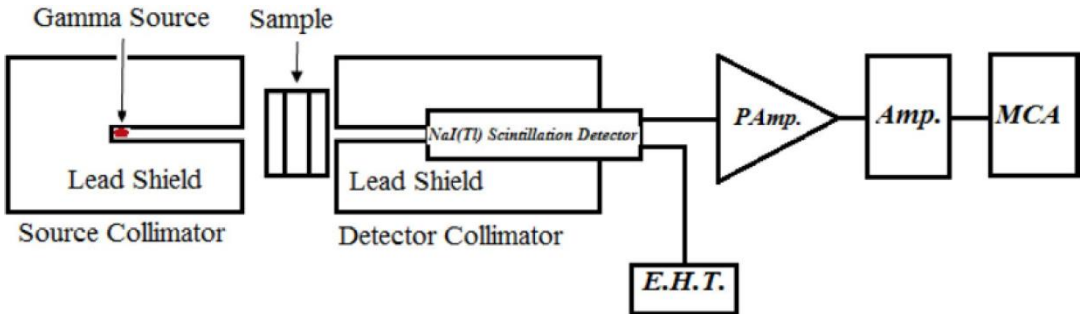

Fig 2: Schematic diagram of experimental setup for gamma ray detection

The comparison between experimental and theoretical data was carried out by using the WinXCom computer program (version 3.1) [32],[33],[34] to calculate the mass attenuation coefficients of γ-rays of such used energies for the studied concrete samples based on the mixture rule of the following equation: (4) Where, (μi/ρi)m is the mass attenuation coefficient for the individual element in each mixture sample, W_i is the fraction weight of the element in each mixture sample.

$$\sigma_{Th} = \sum_i^n W_i (\frac{\mu_i}{\rho_i})_m$$ Eq (4)

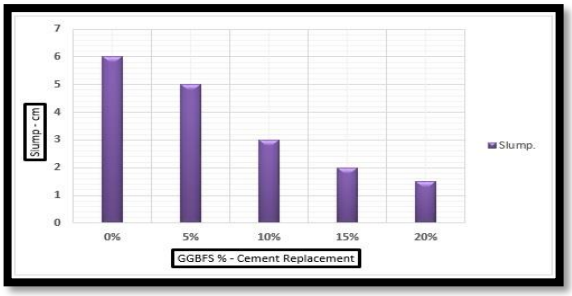

Fig.3: Effect of slag as cement replacement on slump value.

3. Results and Discussion

Fresh Concrete

The slumps of fresh concrete for different mixtures were shown in Fig. 3. It was noticed that the slump test values were decreased with increasing slag content in concrete. This behavior was probably due to the rough texture and high-water absorption of slag particles, leading to low fluidity.

Microstructure (SEM)

Fig. 4 (a-e) shows microstructure of concrete with and without slag. It can be seen that the plain concrete has more voids comparing to concrete with slag. In addition, the figure revealed that the voids decreased with increasing slag content to 15 wt. %. Beyond this value the voids increased again, but still lower than both the plain specimens. On the other hand, Fig. 4 displays that the internal structure of slag concrete was similar to the structure of Portland cement.

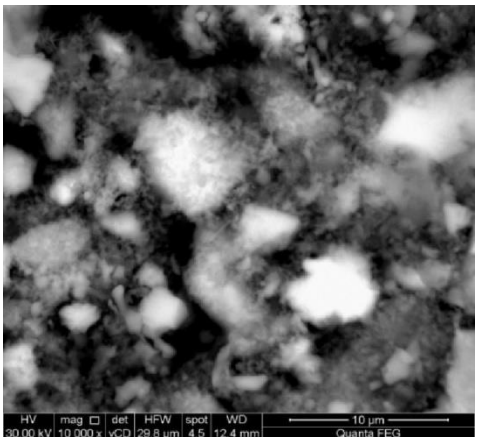

(a)

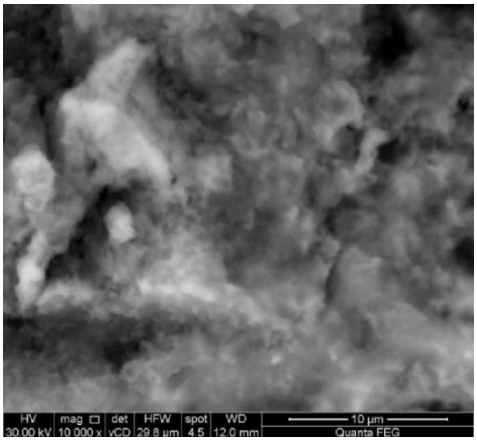

(b)

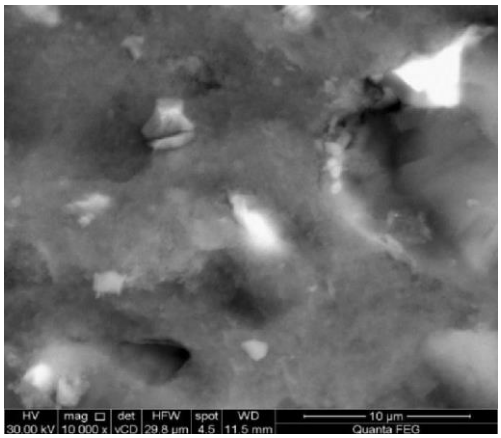

(c)

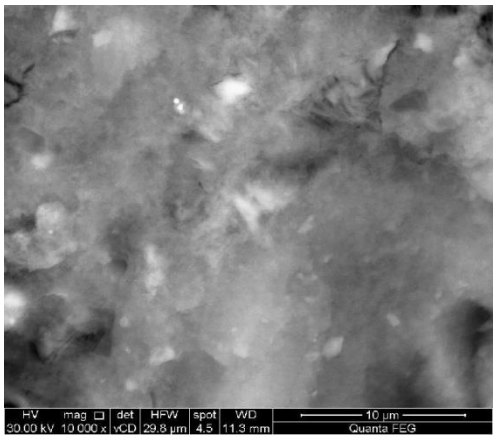

(d)

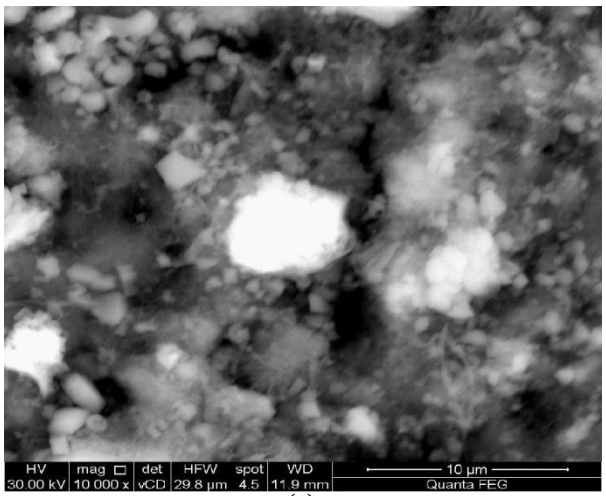

(e)

Fig4: Microstructure of concrete with and without slag as cement. (a) Concrete without slag, (b) 5wt. % slag, (c) 10 wt. % slag, (d) 15wt. % slag and (e) 20wt. % slag

Mechanical properties of hardened concrete

Compressive strength

Fig. 5 presents the compressive strength of concrete with and without slag as cement replacement after 7 and 28 days of curing. The results revealed that the compressive strength for all concrete mixes increased with the curing time. This was mainly attributed to the cement hydration and accumulation of hydration products which close some of available pore spaces in concrete matrix and result in improving the mechanical performance. Furthermore, Fig. 5 indicated that the compressive strength increased by adding slag from 5 % to 15wt% replacements. Beyond this value the compressive strength decreased. This reduction in compressive strength for concrete mix with 20wt% replacement was due to the decrease in the free water content that resulted from the high-water absorption characteristics of arc furnace slag in comparison with sand (see Fig. 4-e). This causes a considerable decrease in the workability of concrete and hence, increases the voids in this mix.

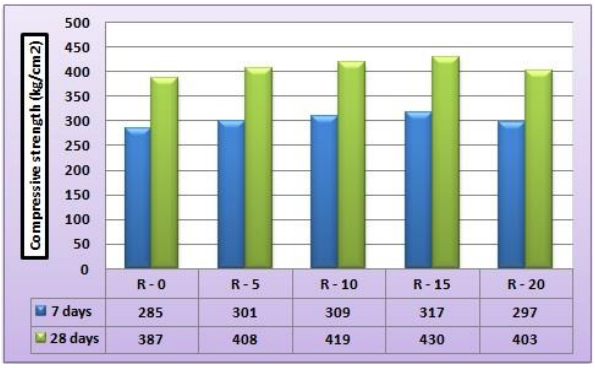

Fig. 5: Effect of slag as a cement replacement on compressive strength of concrete

Splitting tensile strength

Fig. 6 depicts the results for splitting tensile strength of different slag mixes concrete. It was noticed that all slag mixes have gained higher split tensile strength than that of the control mix. However, beyond 15% replacement of cement, the tensile strength decreases, but still more than the control mix. The trend was similar to the trend of compressive strength development of concrete. This behavior was due to decreasing the cementitious material per surface area of fine.

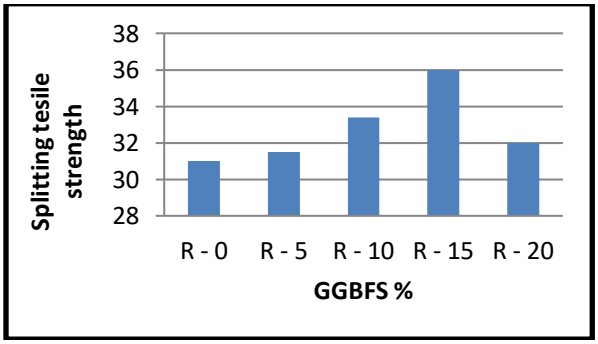

Fig. 6: Effect of slag as a cement replacement on splitting tensile strength of concert

Gamma-rays measurements and calculations

The intensity distribution of gamma rays transmitted through concrete barriers of different thicknesses were measured and plotted for different types of concrete mixes at gamma ray energy lines (662keV). These exponential curves were used to deduce the total linear attenuation coefficients (μ, cm-1) as a slope of these curves. Figs. 7-9 showed the behavior of measured and calculated mass attenuation coefficient (σ, cm2/g) with different thicknesses. The first note of these curves was a good agreement between the measured values of mass attenuation coefficients and that calculated by winXCom computer program(version 3.1), Also, the behavior of all these curves can be interpret by the prominent interaction between the investigated concrete barriers and gamma rays which considered a Compton scattering process as well as less contribution of photoelectric effect in low energies.

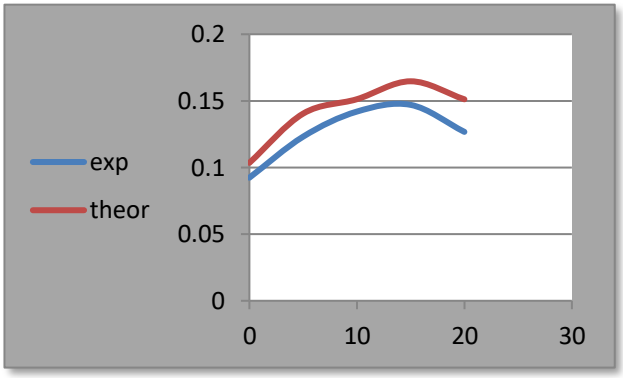

Fig. 7: Mass attenuation coefficients of concrete with slag at 5 cm

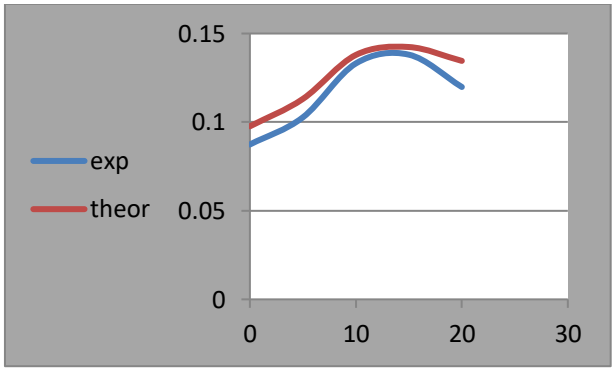

Fig. 8: Mass attenuation coefficients of concrete with slag at 10 cm

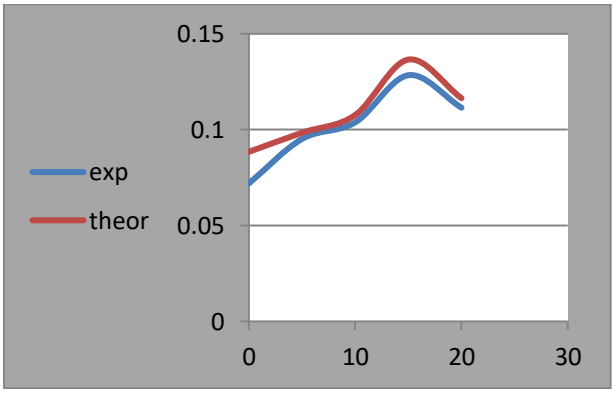

Fig. 9: Mass attenuation coefficients of concrete with slag at 15 cm

Fig.10 shows the comparison between values of mass attenuation coefficients in different types of concrete mixes using gamma ray energies (122 -1332 keV). It can be seen that the values of σ (by cm2/g) were increased by increasing the weight percentage of slag in concrete mixes up to 1173 keV gamma ray energy, which may be attributed to Z-dependence of Compton scattering process in this energy region. While for another gamma ray energies there is a fluctuation distribution of values of mass attenuation coefficient. This behavior is in agreement with work of El-Shazl and Sadawy [35] how used blast furnace slag as fine aggregate.

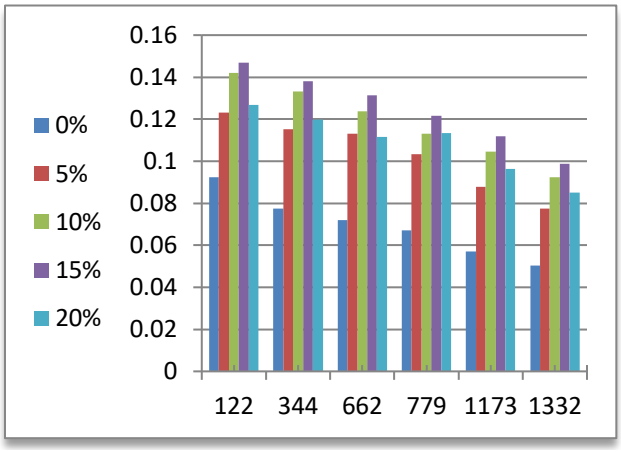

Fig 10: Comparison between mass attenuation coefficients of investigated concrete mixes with different gamma ray energies.

Neutron measurements

The values of removal cross-sections of total slow neutrons (Kn1) (primary slow as well as slowdown in the studied concrete mixes), slow (Kn2), and neutron with energy greater than 10 keV (Kn3) were deduced from attenuation curves and shown in Table3. It was observed that, the values of macroscopic cross-sections of slow neutrons in all types of concrete under investigation were the biggest values of the others neutron energies. This behavior of slow neutrons may be attributed to elastic scattering of slow neutron with light elements in all types of concrete mixes. Also, it was noticed that the values of macroscopic cross-sections of total slow neutron slightly increasing than that of neutron with energy greater than 10 keV in all concrete mixes. This behavior may be attributed to the competition between absorption process and slowdown process which takes place in the case of total slow neutron, while in the case of neutron with energy greater than 10 keV the only slow down process that appear. (Note that, about 23% of neutron energies emitted from ^{241}Am-Be neutron source is considered slow neutron). Also, it was observed from Table3 that the values of macroscopic cross-sections of all used neutron energies almost constant with increasing the percentage weight of slag in concrete mixes. This result can be interpreted as, the addition of slag up to 20 wt% as a cement in the concrete decreased the percentage of SiO2.

Table 3: Macroscopic cross-sections of concrete mixes at different neutron energies

k	Macroscopic cross-section, cm-1				
	0%	5%	10%	15%	20%
k_{n1}	0.038	0.041	0.039	0.038	0.037
k_{n2}	0.077	0.078	0.077	0.076	0.076
k_{n3}	0.031	0.033	0.034	0.034	0.033

4. Conclusions

- ✓ Slump test values were decreased with increasing slag content in concrete.
- ✓ The mechanical properties of concrete were increased with increasing electric arc furnace slag up to 15 wt. % compared to mix control sample
- ✓ A good agreement between the measured values of mass attenuation coefficients and that calculated by winXCom computer program(version 3.1)
- ✓ 15wt % of arc furnace slag as a cement in concrete was the optimum percentage for the values of mass attenuation coefficients of the most investigated γ-ray energy lines in concrete maxis.
- ✓ There is no a significant variation of the values of Σ for all used neutron energies by adding a different percentage of slag as cement in concrete.

5. References

1 Pomaro, B.; Salononi, V.A.; Gramegna, F.; Prete, G.; Majorana, C.E. Radiation damage evaluation on concrete within a facility for selective production of exotic species (SPES project), Italy. J. Hazad.Mater. 2011, 194, 169-177.

2 Gencel, O. Effect of elevated temperatures on mechanical properties of high-strength concrete containing varying proportions of hematite, Fire. Mater. 2012, 36, 217-230.

3 Chitralekha; Kerur, B.R.; Lagare, M.T.; Nathuram, R.; Sharma, D.N. Mass attenuation coefficients of saccharine for low-energy X-rays, Radiat.Phys. Chem. 2005, 72, 1-5. 318

4 El-Khayatt, A.M. Radiation shielding of concretes containing different lime/silica ratios, Ann. Nucl. 319 Energy 2010, 37, 991-995.

5 Agosteo, S.; Magistris, M.; Mereghetti, A.; Silari, M.; Zajacova, Z. Shielding data for 100-250 MeV proton accelerators: Attenuation of secondary radiation in thick iron and concrete/iron shields, Nucl. Instrum. Methods Phys. Res. B. 2008, 266, 3406-3416.

6 ACI 304R Guide for Measuring, Mixing, Transporting and Placing Concrete.

7 Xi, S.; Bourham, M.; Rabiei, A. A novel ultra-light structure for radiation shielding, Mater. Des. 2010, 31, 2140-2146.

8 Akkurt, I.; Basyigit, C.; Kilincarslan, S.; Mavi, B.; Akkurt, A. Radiation shielding 326 of concretes containing different aggregates, Cem. Concr. Compos. 2006, 28, 153- 157.

9 Kharita, M.H.; Takeyeddin, M.; Alnassar, M.; Yousef, S. Development of special radiation shielding concretes using natural local materials and evaluation of their shielding characteristics, Prog. Nucl. Energy. 2008, 50, 33-36.

10 Akkurt, I.; Akyildirim, H.; Mavi, B.; Kilincarslan, S.; Basyigit, C. Photon attenuation coefficients of concrete includes barite in different rate, Ann. Nucl. Energy. 2010, 37, 910-914.

11 Mesbahi, A.; Azarpeyvand, A.; Shirazi, A. Photoneutron and backscattering in high density concretes used for radiation therapy shielding, Ann. Nucl. Energy. 2011, 38, 2752-2756.

12 Maslehuddin, M.; Naqvi, A.A.; Ibrahim, M.; Kalakada, Z. Radiation shielding properties of concrete with electric arc furnace slag aggregates and steel shots, Ann. Nucl. Energy. 2013, 53, 192- 196.

13 Akkurt, I.; Akyildirim, H.; Mavi, B.; Kilincarslan, S.; Basyigit, C. Gamma-ray shielding properties of concrete including barite at different energies, Prog. Nucl. Energy. 2010, 52, 620-623.

14 Rezaei Ochbelagh, D.; Azim Khani, S.; Gasemzadeh Mosavinejad, H. Effect of gamma and lead as an additive material on the resistance and strength of concrete, Nucl. Eng. Des. 2011, 241, 2359-2363.

15 Sharma, A.; Reddy, G.R.; Varshney, L.; Bharathkumar, H.; Vaze, K.K.; Ghosh, A.K; Kushwaha, H.S.; Krishnamoorthy, T.S. Experimental investigations on mechanical and radiation shielding properties of hybrid lead-steel fiber reinforced concrete, Nucl. Eng. Des. 2009, 239, 1180-1185.

16 Turkmen, I.; Ozdemir, Y.; Kurudirek, M.; Demir, F.; Simsek, O. Calculation of radiation attenuation coefficients in portland cements mixed with silica fume, blast furnace slag and natural zeolite, Ann. Nucl. Energy. 2008, 35, 1937–1943.

17 Singh, C.; Singh, T.; Kumar, A.; Mudahar, G.S. Energy and chemical composition dependence of mass attenuation coefficients of building materials, Ann. Nucl. Energy. 2004, 31, 1199–1205.

18 Alam, M.N.; Miah, M.M.H.; Chowdhury, M.I.; Kamal, M.; Ghose, S.; Rahman, R. Attenuation coefficients of soils and some building materials of Bangladesh in the energy range 276-1332 keV, Appl. Radiat. Isot.2001, 54, 973–976.

19 Salinas, I.C.P.; Conti, C.C.; Lopes, R.T. Effective density and mass attenuation coefficient for building material in Brazil, Appl. Radiat. Isot. 2006, 64, 13- 18.

20 Medhat, M.E. Gamma-ray attenuation coefficients of some building materials available in Egypt, Ann. 355 Nucl. Energy. 2009, 36, 849-852.

21 Faraone, N.; Tonello, G.; Furlani, E.; Maschio, S. Steelmaking slag as aggregate for mortars: Effects of particle dimension on compression strength, Chemosphere. 2009, 77, 1152-1156.

22 Qasrawi, H.; Shalabi, F.; Asi, I. Use of low CaO unprocessed steel slag in concrete as fine aggregate. Constr, Build. Mater. 2009, 23, 1118-1125.

23 Correia, S.L.; Souza, F.L.; Dienstmann, G.; Segadaes, A.M. Assessment of the recycling potential of fresh concrete waste using a factorial design of experiments, Waste Manage. 2009, 29, 2886-2891.

24 Salihoglu, G.; Pinarli, V. Steel foundry electric arc furnace dust management: Stabilization by using lime and portland cement, J.Hazad. Mater. 2008, 153, 1110-1116.

25 Wang, G.; Wang, Y.; Gao, Z. Use of steel slag as a granular material: Volume expansion prediction and usability criteria, J. Hazad. Mater. 2010, 184, 555- 560.

26 Wang, G. Determination of the expansion force of coarse steel slag aggregate, Constr. Build. Mater. 2010, 24, 1961-1966.

27 Adegoloye, G.; Beaucour, A.L.; Ortola, S.; Noumowe, A. Concretes made of EAF slag and AOD slag aggregates from stainless steel process: Mechanical properties and durability, Constr. Build. Mater. 2015, 76, 313-321.

28 Roslan, N.H.; Ismail, M.; Abdul-Majid, Z.; Ghoreishiamiri, S. Performance of steel slag and steel sludge in concrete, Constr. Build. Mater. 2016, 104, 16-24.

29 J. S. Lilley, Nuclear physics principle and applications, John Wiley & Sons, Ltd, 2002.

30 Vishwanath P. Singh and N.M. Badiger, ―Gamma ray and neutron shielding properties of some alloy materials‖, Annals of Nuclear Energy, 64, pp. 301– 310, 2014.

31 Burcu AKÇA and Salih Zeki ERZENEOĞLU, ―Measurement of Linear Attenuation Coefficients of Compounds of Some Essential Major Elements‖, Journal of Multidisciplinary Engineering Science and Technology (JMEST), 3(6), pp. 5003-5006, 2016.

32 Vishwanath P. Singh, M.E. Medhat, and S.P. Shirmardi, ―Comparative studies on shielding properties of some steel alloys using Geant4, MCNP, WinXCOM and experimental results‖, Radiation Physics and Chemistry, 106, pp. 255–260, 2015.

33 AlySaeed, R.M. El shazly, Y.H. Elbashar, A.M. Abou El-azm, M.M. El-Okr, M.N.H. Comsan, A.M. Osman, A.M. Abdal-monem, A.R. El-Sersy, ―Gamma ray attenuation in a developed borate glassy system‖, Radiation Physics and Chemistry, 102, pp. 167–170, 2014.

34 Gerward, L., Guilbert, N., Jensen, K.B., Levring, H., ―X-ray absorption in matter Reengineering XCOM‖, Radiat. Phys. Chem., 60, pp. 23–24, 2001.

35 R. M. El Shazly, M.M. Sadawy- Effect of Slag as a Fine Aggregate on Mechanical, Corrosion, and Nuclear Attenuation Properties of Concrete, International Journal of Scientific Engineering and Research (IJSER) ISSN (Online): 2347-3878Volume 5 Issue 7, July 2017